SIZE EFFECT IN PAPER FIBER-REINFORCED GYPSUM PANELS UNDER IN-PLANE BENDING

Wolfgang Klöck
Engineer
Department of Timber Construction

and

Simon Aicher
Head
Division of Wood and Fire Behaviour
MPA University of Stuttgart
Otto-Graf-Institute
Pfaffenwaldring 4
70569 Stuttgart, Germany

(Received February 2003)

ABSTRACT

This paper discusses the influence of the size effect on the in-plane bending strength of paper fiber-reinforced gypsum panels. The incombustible composite material consists of randomly dispersed, recycled paper fibers embedded in a gypsum matrix. The brittleness of the material is considerably lower as compared to classical gypsum board. The panels are primarily employed in building industry for sheathing and bracing of timber and steel frame wall elements and for flooring applications.

The size effect study was performed on 3-point bending specimens that were identical in thickness, being 12.5 mm; depth however, with seven different dimensions was ranging from 10 to 320 mm. The experiments, for which the sample size was nominally eleven specimens per depth, were performed with a constant cross-head rate until complete separation of the specimens. The load-deflection curve was completely stable throughout the loading, even on the descending load branch beyond peak load. Thus, paper fiber-reinforced gypsum panels represent a strain-softening material. The nonlinearity of the stress-displacement curves becomes more accentuated near peak load for smaller depths. This can be explained by the increasing ratio of the fracture process zone length to the specimen depth.

The tests revealed a nonlinear strength reduction with increasing specimen size, which was fitted by a one-parameter power law equation based on a Gauss-Newton approach. The statistical analysis of the fitted size effect curve verified the basic assumptions of normally distributed residuals and of a constant variance of the different samples. Furthermore, analysis of the variance revealed the adequacy of the chosen model function. For statistical inference on the population, confidence intervals are given for the model parameter and for the mean and individual strength values.

Keywords: Paper fiber-reinforced gypsum panels, in-plane bending strength, size effect, strain softening.

INTRODUCTION

The objective of the investigation presented was to verify quantitatively the assumed size effect in paper fiber-reinforced gypsum panels under in-plane bending loading. The assumption of a pronounced size effect for paper fiber-reinforced gypsum panels in general, which has not been verified so far in the literature, emanated from an earlier study focussing on the fracture mechanics properties of this material at in-plane bending, e.g. fracture process zone length (Aicher and Klöck 2000). The investigations revealed that the material is characterized by strain-softening. The found quantities of the

Wood and Fiber Science, 37(3), 2005, pp. 403–412

critical crack extension and of the limit value of the fracture process zone length (about 20 mm) strongly suggest a nonlinear size effect with increasing specimen depth.

In the evaluation of the test data presented, emphasis was laid on statistical aspects of the applied size effect model in order to enable an unbiased inference on the population of the material examined.

THE COMPOSITE MATERIAL—PAPER FIBER-REINFORCED GYPSUM PANEL

Paper fiber-reinforced gypsum panels may be classified as a short-fiber composite material as opposed to a long-fiber composite material. The anorganic matrix material is gypsum, which may be natural gypsum or often artificial gypsum gained from washing of sulfuric gases from coal power plants. The organic paper fibers are cellulose paper fibers gained from recycled newsprint and waste paper. The length of the individual fibers ranges from about 1 to 5 mm. The fibers are quite interwoven so that the fiber material could perhaps more accurately be termed as a "fiber fluff". In the finished panel, the fibers are oriented predominantly (roughly 80% to 90%) planar in the panel plane. The in-plane stiffness and strength properties show a slight orthotropy, whereby the values perpendicular to the panels' production direction are roughly 5% higher. The fiber volume fraction ranges from about 16 to 20%. The maximum fiber volume fraction is bound to the target requirement of incombustibility of the composite material limiting the proportion of the highly inflammable fibers.

Paper fiber-reinforced gypsum panels in general have a density in the range of 1050 to 1250 kg/m^3 and are primarily manufactured in thicknesses of 10, 12.5, 15, and 18 mm. Special panels for double-floors are manufactured with a thickness of 36 mm and have a density of about 1400 kg/m^3. For further manufacturing and technical details and for new developments, see e.g. Miller and Lynn 1998; Hummel 2000.

Important features of the material are: 1) its incombustibility, reflected by a Euroclass B rating for reaction to fire, 2) the high environmental friendliness of both of its easily recyclable and disposable constituents, and 3) a considerably decreased brittleness compared to usual gypsum board due to the dispersed fibers.

The material has gained success as an improved substitute for gypsum board; recently, the first European Technical Approval has been issued (DIBt 2004). In structural applications, it is used primarily for sheathing and bracing of timber and steel-framed wall constructions and for flooring applications. The use of the incombustible panels in point- or line-supported double-floors, for which it is subjected to out-of-plane bending, represents an application beyond the material limits of conventional gypsum board.

At present, the North (U.S.) American acceptance criteria for nonpaper-faced fiber-reinforced gypsum panels used as an alternate to gypsum board, as given in ICBO AC 158 (1999), and ASTM standards C 79 and C 473 (ASTM 2004; 2003b) do not cover any in-plane material tests and respective requirements. The same applies to the provisions given in ASTM C 1278 (2003b) defining the Standard Specification for Fiber-reinforced Gypsum Panels.

In Europe, the use of the material class considered for structural applications/sheathing is subject to National or European Technical Approvals. The latter have to be derived on the basis of a so-called European Common Understanding of Assessment Procedure (CUAP) specifying the necessary verification methods. The CUAP on "Large-sized fiber gypsum panels used for walls of prefabricated houses" (DIBt 2002), which applies exclusively to panels reinforced with cellulose fibers of a volume fraction $\leq$20%, prescribes in-plane tension and compression strength and stiffness tests according to European Standard EN 789 (CEN 2003).

Validated correlations between in-plane tension, compression and bending properties, still to be established for this type of material, might allow in the future the testing of in-plane strength and stiffness characteristics exclusively by means of edgewise bending tests.

SPECIMENS AND TEST METHOD

The size effect study with 3-point bending specimens of considerably different sizes, yet of similar in-plane geometry (2D-similarity), was conducted with seven different specimen depths sampled from a total of ten panels. The depth of the specimens was always parallel to the production direction of the panels. The nominal thickness of the investigated panel material, conforming to the product requirements specified in the technical approval (DIBt 1998), was 12.5 mm. The oven-dry density was 1182 ± 16.4 kg/m^3 (C.O.V. = 1.4%). Before testing, the specimens were conditioned for 20 days in a constant climate of 20°C/65% relative humidity. The mean moisture content of the specimens, determined by the oven-dry method immediately prior to testing, was 1.3 ± 0.13%; this is within the estimated range for this type of material.

The span-to-depth ratio of the specimens was L_δ/ D = 6, and the ratio of total specimen length to specimen depth was L / D = 7. The seven depths investigated were 10, 20, 40, 80, 160, 240, and 320 mm. Each of the seven depths investigated in an individual test series is comprised nominally of 11 specimens. The test series with depths of 10 and 20 mm consisted of only 10 specimens. In the case of the largest specimen size, D = 320 mm, only six specimens were tested (see Table 1).

Figure 1 shows the scheme of the test set-up. In order to achieve the best possible 2D-similarity of the specimens and of the local loading conditions, the bearing plates and rollers at the support and loading points were scaled with regard to the specimen depths. All bending specimens, except those with the very small depths of 10 and 20 mm, were braced to prevent lateral buckling.

The tests were performed under displacement control with a constant loading rate, which was adjusted according to the specimen size to obtain failure within 300 ± 60 s. The loading rate varied from 0.25 to 1.5 mm/min for specimen depth D = 10 and 320 mm, respectively. The displacement, i.e. the mid-span deflection, was measured at the bending compression edge by means of two LVDT's placed on both sides of the specimen.

Bending strength f_m was computed as

$$f_m = \frac{3P_u L_s}{2BD^2} \tag{1a}$$

$$\text{where } P_u = P_u^0 + P_{ae} + mg\,\frac{2L_s - L}{2L_s} \tag{1b}$$

In Eq. (1b), the quantity P_u^0 represents the measured maximum load displayed by the test machine, and P_{ae} stands for the weight of the ancillary equipment (loading plate and ball) resting on the specimen. The third term, in which m is the mass of the individual specimen and g is the acceleration of gravity, accounts for the self-weight of the specimen. For the span ratio L_s : L = 6 : 7, the third term simplifies to m · g · 5/12.

TEST RESULTS AND DISCUSSION

Prior to a discussion of the size dependency of the strength values, the load-deflection and frac-

TABLE 1. *Compilation of bending strength results of all test series with different specimen sizes.*

Test Series No.	Specimen Depth D	Span L_x	No. of Specimens n	Bending Strength f_m			
				Mean $\bar{x}$	Std. dev. ± s	C.O.V.	x_{min}
—	mm	mm	—	N/mm^2	N/mm^2	%	N/mm^2
I	10	60	10	5.89	0.44	7.4	5.13
II	20	120	10	5.62	0.43	7.7	5.00
III	40	240	11	5.06	0.43	8.6	4.32
IV	80	480	11	4.78	0.22	4.6	4.45
V	160	960	11	4.27	0.20	4.6	4.06
VI	240	1440	11	4.00	0.30	7.4	3.55
VII	320	1920	6	3.82	0.29	7.5	3.37

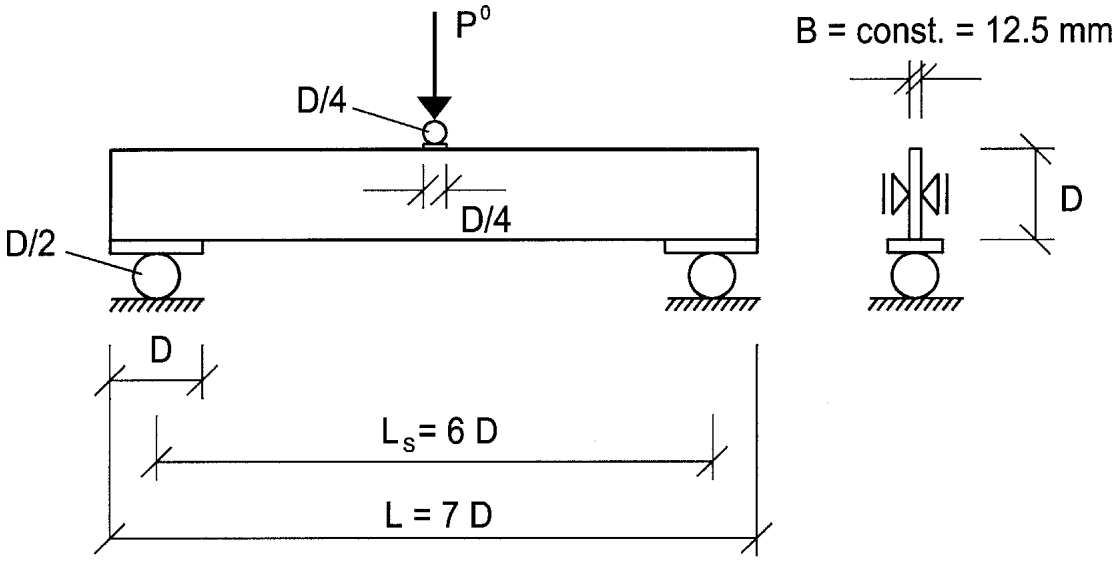

FIG. 1. Scheme and dimensions of test set-up.

ture behavior shall be briefly examined. The fracture appearance is characterized by a single crack, running rather parallel to depth. The location of the crack on-set is very close to maximum bending moment at mid-span; the off-set hereof is in the range of a few to maximally about 10 mm. The crack path, although globally rather straight is in general slightly meandering within the aforementioned absolute deviation range. To the naked eye, the crack on-set and its further propagation are visible only beyond peak load (see below).

All specimens, independent of size, failed in a stable manner. This means that the load-deflection behavior beyond peak load was completely stable on the descending load path until zero load was reached at very large displacements when the specimens finally separated into two parts.

Figure 2 shows representative bending stress-displacement curves of specimens of the different sizes investigated. To enable a comparison between the different sizes, the absolute displacement, i.e. mid-span load point deflection u, 'is normalized by the specimen depth D. This is a typical scaling procedure in fracture mechanics evaluations (Bazant and Planas 1998). It can be seen that the pronounced softening behavior of the very small specimens changes continuously to a more brittle behavior at larger specimen sizes. (Note: The same effect is visible without normalization of the unscaled load-deflection curves, not shown here). The effect described is the apparent result of the increasingly reduced ratio of the fracture process zone length to specimen depth.

The linear elastic part of the load-deflection curve reached up to about 75% of the ultimate load P_u for the smallest depth (D = 10 mm). For the largest size, D = 320 mm, the nonlinearity started at about 95 % of P_u. The transition from the linear stiffness range to progressive damage with decreasing stiffness is characterized in general, except for the smallest specimen size D = 10 mm, by a very small pre-peak load drop. It can be assumed that the load drop is associated with a minor macro-crack initiation, which is, however, invisible by naked eye.

The pre-peak instability feature is probably due to a critical ratio of specimen size to fracture process zone length and/or a critical value of stored elastic energy.

Empirical cumulative frequencies (i-0.5)/n (i = 1 . . . n: rank of strength values sorted in ascending order) for bending strengths of all specimens of the individual test series are shown in

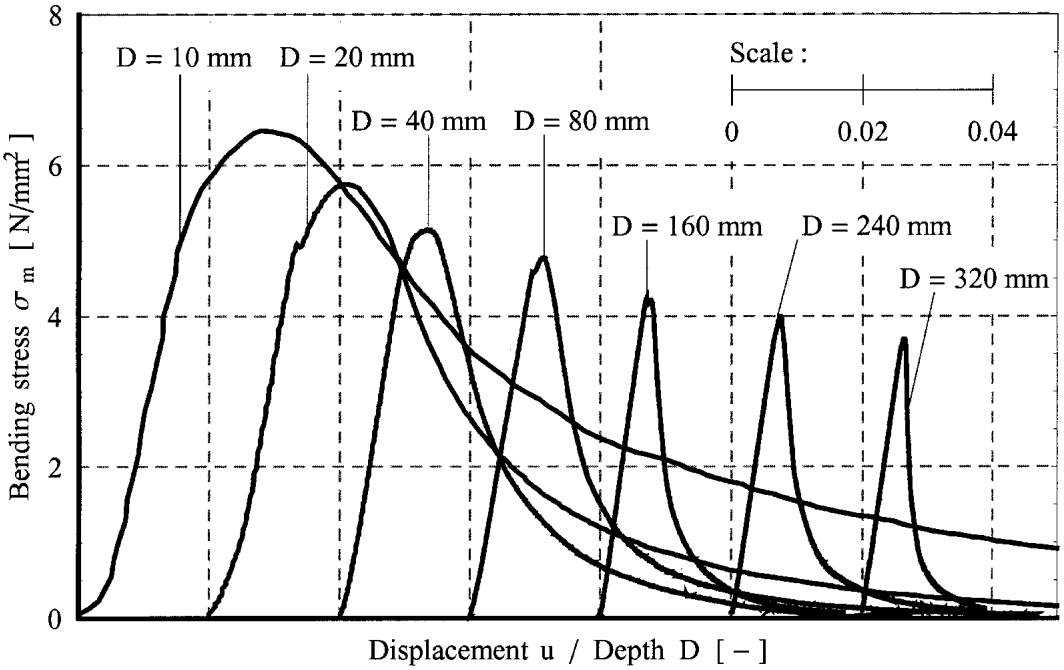

FIG. 2. Curves of bending stress versus mid-span deflection (depth-normalized) of different-sized specimens until complete failure.

Fig. 3; further, the fitted cumulative normal distribution functions are given. Table 1 provides the mean bending strength for each test series and, furthermore, standard deviations, coefficients of variation (COVs), and the minimum strength values.

SIZE EFFECT MODEL

The apparent strong dependence of the bending strength f_m on specimen depth D can be described by different mathematical functions with or without physical background. In the following discussion, the size effect model will be restricted to a one-parameter power law equation

$$f_m = f_{m,D_0}\left(\frac{D_0}{D}\right)^{\frac{1}{m}} \tag{2}$$

where D_0 represents an arbitrarily chosen reference depth, f_{m,D_0} is the corresponding mean bending strength, and m is the size effect parameter.

For the determination of the size effect parameter m, first the individual test results are fitted by an unweighted least squares method using the Gauss-Newton approach. The nonlinear regression model may be written in general terms as

$$\mathbf{Y} = f(\mathbf{x},\boldsymbol{\theta}) + \mathbf{Z} \text{ where } \mathbf{Z} \sim N(\mathbf{0}, \sigma^2 \mathbf{I}) \tag{3a, b}$$

The response vector $\mathbf{Y} = f_m$ according to Eq. (3a) consists of the deterministic model function f(X,θ), here given by Eq. (2) with $\mathbf{x} = D$ and $\boldsymbol{\theta} = m$ and of the stochastic part, the residual vector **Z.** Equation (3b) presents the basic assumption of the unweighted least-squares estimate that the vector of residuals is normally distributed around a mean value of zero and shows a constant variance σ^2; **I** is the identity matrix.

The least-squares minimization ($\mathbf{y} = f_m$) of all (N = 70) individual strength data y_i by Eq. (3) delivers the point estimate $\hat{m} = 8.13$. The reference size in Eq. (2) was chosen as $D_0 = 160$ mm and hence $f_{m,D_0} = 4.27$ N/mm^2 as shown in Table 1.

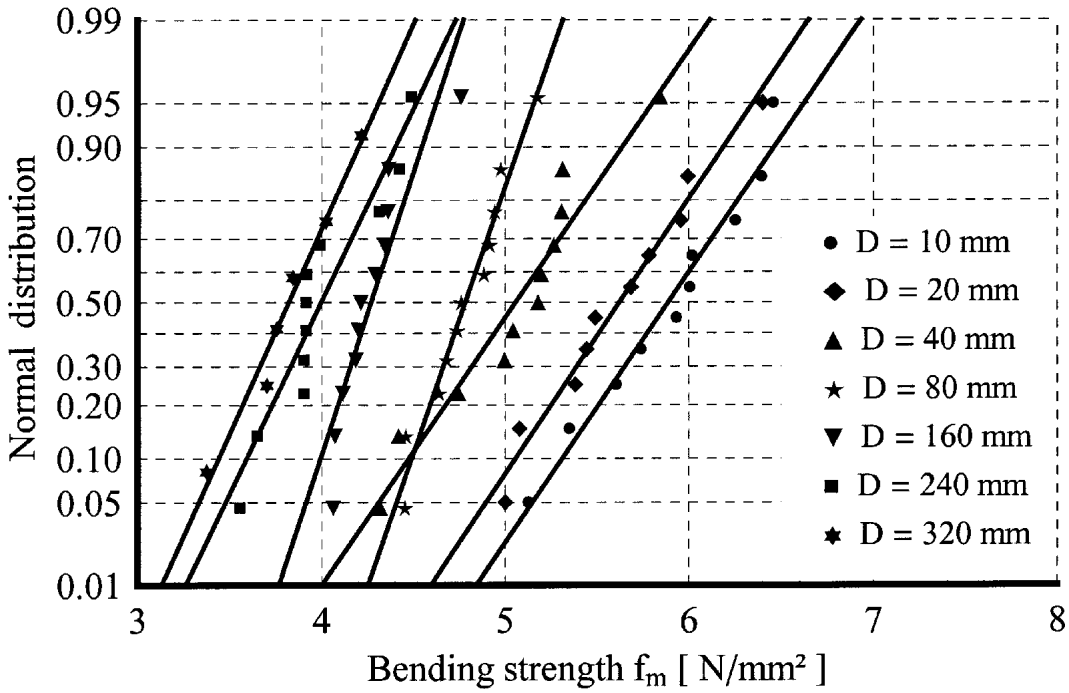

FIG. 3. Cumulative failure frequencies and fitted cumulative normal distribution functions of bending strengths of all data sets with different specimen sizes.

Figure 4 depicts the derived mean power law size effect curve (D in mm)

$$f_m = 4.27 \left(\frac{160}{D}\right)^{\frac{1}{8.13}} [N/mm^2] \qquad (4)$$

together with the individual experimental bending strength results. The inserted graph shows the histogram of the actual residuals and their normal probability density.

The unweighted residual sum of squares of the point estimate is $S(\hat{m}) = 8.011$ yielding an estimated constant variance of the residuals

$$s^2 = S(\hat{m})/(N - P) = 0.116 \qquad (5)$$

where $P = 1$ is the number of parameters of the model function.

Verification of normal distribution of residuals and of constance of variance

A common check of the initially assumed normal distribution of the residuals $\hat{z}_i$ is a plot of the standardized residuals

$$\hat{z}_{i,stand} = \hat{z}_i / s\sqrt{1 - h_{ii}} \qquad (6)$$

sorted in ascending order with respect to the normal quantile. In Eq. (6), s is the standard deviation of the residuals, and the h_{ii} are the i-th diagonal elements of the "hat" matrix $\mathbf{H} = \hat{\mathbf{Q}}_1 \hat{\mathbf{Q}}^T$. For discussion of $\hat{\mathbf{Q}}$, see e.g. Bates and Watts (1988). Provided, that the employed model function and the assumption of normally distributed residuals are correct, the plot should result in a fairly straight line. It is obvious from Fig. 5 that this criterion is fulfilled.

The prerequisite of the unweighted least-squares estimate, that the individual data sets have a constant variance (homoscedasticity), can be verified by a plot of the standardized residuals with respect to the predicted response (Eq.(4)). The graph should, and actually does result in a rather uniform band of the standardized residuals $\hat{z}_{i,stand}$ around the value zero (Fig. 6). A quantitative proof of the admissibility of neglecting the actual variances of the individual data sets can be shown by a weighted least-

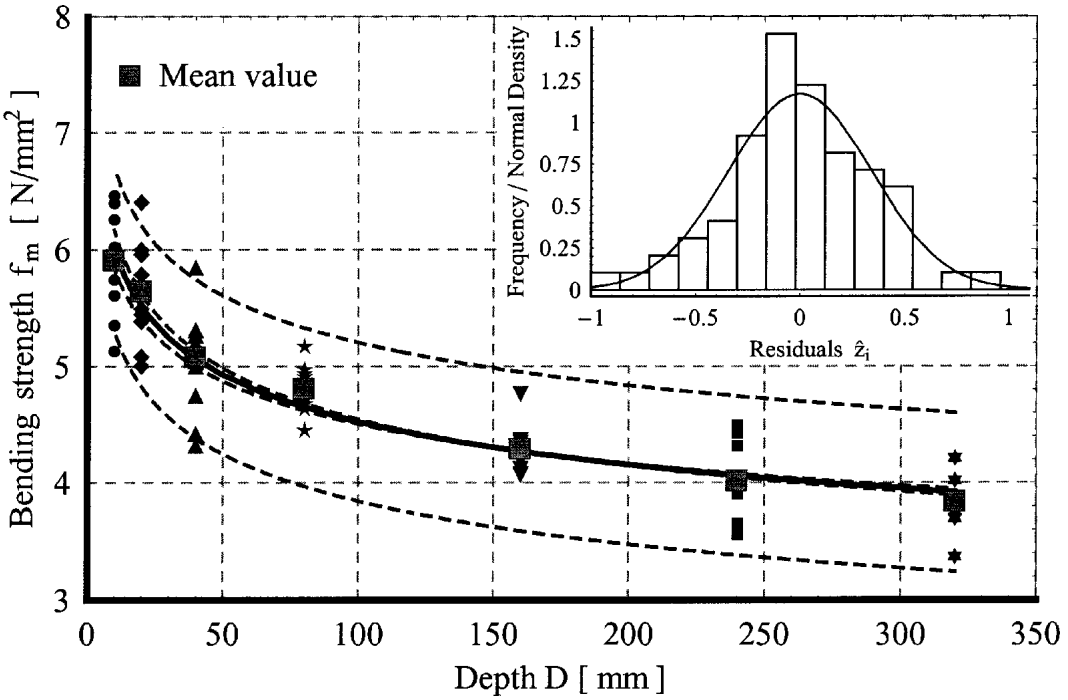

FIG. 4. Dependency of bending strength results on specimen size and fitted one-parameter power law size effect curve, as well as approximate confidence bands (significance level $\alpha = 0.05$) for mean (dashed curves) and individual (dashed outer curves) values of the population.

squares fit. The so-obtained exponent of the model function $\hat{m}_w = 7.94$ differs only marginally (2%) from $\hat{m} = 8.13$ of the unweighted least-squares estimate.

Analysis of variance

The adequacy of a chosen model function, here Eq. (2), for fitting of the experimental data is generally assessed by an analysis of variance (ANOVA) test. The results of the ANOVA are stated in Table 2. For a significance level of $\alpha = 0.05$ a c-value of 2.25 is obtained, indicating (F Ratio $= 0.788 < 2.25$) adequacy of the chosen model function.

INFERENCE ON THE POPULATION

In general, the expected response vector $\boldsymbol{\eta}(\boldsymbol{\theta}) = f(x_i,\boldsymbol{\theta})$ forms a P-dimensional expectation surface in the N-dimensional response space. Here, the statistical inference on the population was performed by a linear approximation (first-order Taylor series) of the expectation surface $\boldsymbol{\eta}(\boldsymbol{\theta})$ in the optimum point $\boldsymbol{\eta}(\hat{m})$ characterized by being closest to the data vector **y.** In the given case, due to P = 1, vector $\boldsymbol{\eta}(m)$ represents a parametic curve.

Approximate confidence interval of $\hat{m}$

The 100(1-α)% approximate confidence interval of parameter $\hat{m}$ of the model function can be generally expressed as

$$\hat{m} \pm se(\hat{m}) \cdot t(N - P;\, 1 - \alpha / 2) \qquad (7)$$

where se($\hat{m}$) is the approximate standard error of the assumed normally distributed parameter values around the expectation value $\hat{m}$ and t stands for the quantile of Student's t-distribution with N-P degrees of freedom. Here, the approximate $\hat{m}$-confidence interval evolves as (significance level $\alpha = 0.05$) $7.48 \leq \hat{m} = 8.13 \leq 8.78$.

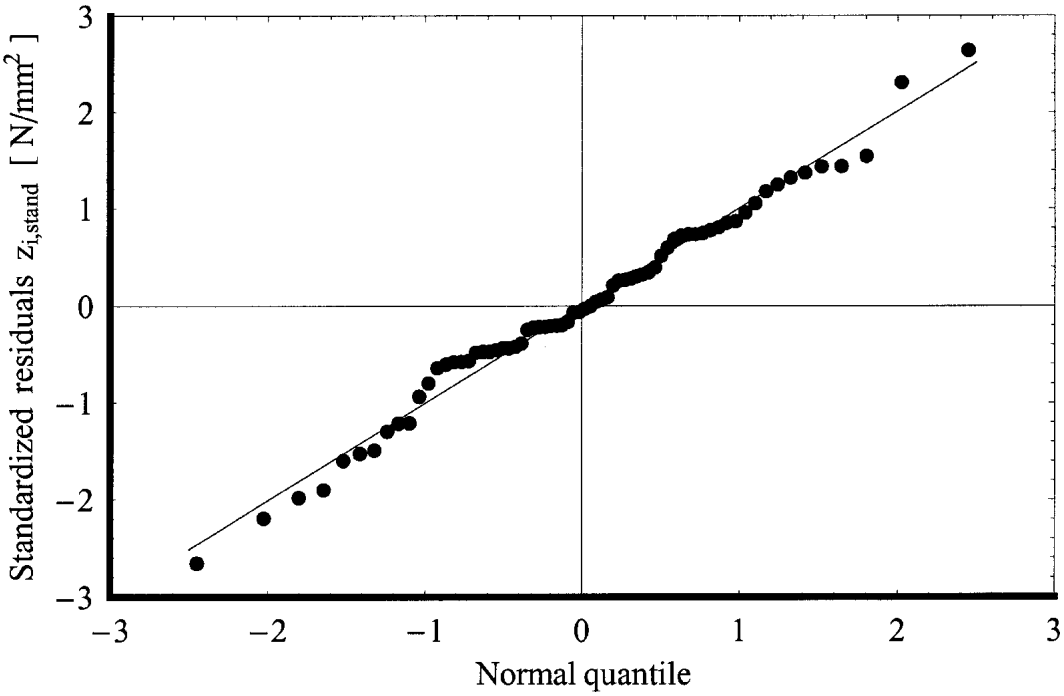

FIG. 5. Plot of standardized residuals versus the normal quantile (Note: The straight line in the plot represents a fit through the standardized residuals).

Approximate confidence bands

The 100(1-α)% approximate confidence bands for the mean values of the population are

$$f(\mathbf{x}, \hat{m}) \pm s\sqrt{\mathbf{v}^{\mathbf{T}}(\hat{\mathbf{R}}_{\mathbf{1}}^{\mathbf{T}}\,\hat{\mathbf{R}}_{\mathbf{1}})^{-\mathbf{1}}\,\mathbf{v}} \cdot \cdot \sqrt{P \cdot F(P, N-P;1-\alpha)} \quad (8)$$

where v represents the derivative matrix at the optimum point $\boldsymbol{\eta}(\hat{m})$, $\hat{\mathbf{R}}_1$ is a matrix obtained from the *QR* decomposition of **v** and *F* stands for the quantile of Fisher's *F*-distribution. Figure 4 shows that the confidence bands of the means (dashed curves) deviate only very slightly from each other and prevailingly encompass the experimental means ($\alpha = 0.05$). So, the derived model function (Eq. 2) represents within the 95% confidence limits a reliable estimate of the mean size effect curve for the in-plane bending strength of the material under consideration. In addition, Fig. 4 shows the confidence bands for the individual values (dashed outer curves).

CONCLUSIONS

The experimental investigation presented reports on a size effect study of in-plane bending strength of paper fiber-reinforced gypsum panels. The experiments with 2-dimensionally scaled, 3-point bending specimens of constant thickness (12.5 mm) were performed with seven samples, each with nominally 11 specimens. The respective cross-section depths varied from 10 to 320 mm. The load-deflection curves were characterized by increasing nonlinearity in the near peak regime, quasi-ductility at peak load, and stable load-bearing behavior on the descending load branch. Ultimate failure, with separation of the specimens into two halves, was obtained at zero load. A slightly increasing "brittleness" was observed with increasing specimen size. This is most likely related to the reducing ratio of the fracture process zone length to specimen depth. The constitutive behavior of the material can be termed as strain-softening which, in general, is

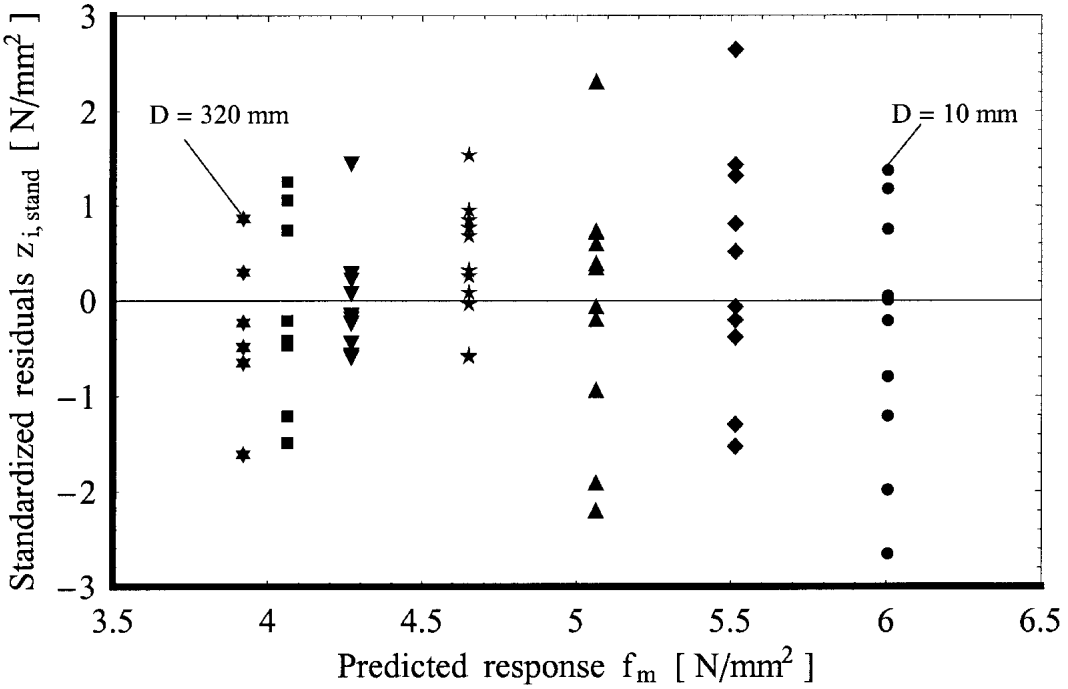

FIG. 6. Plot of standardized residuals versus the predicted response.

TABLE 2. *Results of analysis of variance (ANOVA).*

Source	Degrees of Freedom (DOF)	Sum of Squares	Mean Squares	*F* Ratio
Lack of fit	R−P = 6	$S_1(\hat{m}) = 0.559$	0.0932	0.788
Replication	N−R = 63	$S_2(\hat{m}) = 7.452$	0.1183	—
Residuals	N−P = 69	$S(\hat{m}) = 8.011$	0.1161	—

associated with high energy dissipation (damage) capacity.

A significant size effect on the bending strength was observed. The reduction of mean strength from the smallest to the largest specimen size was 35%. For description of the size effect, a one-parameter power law was fitted to the unweighted experimental data using the Gauss-Newton approach. The assumptions of normally distributed residuals and constant variance of the samples with different depths were proven. The analysis of variance revealed the adequacy of the chosen model function. The presented confidence intervals of mean and individual values of the investigated samples indicate the range for the population of this strain-softening cellulosic short-fiber composite material.

The quantification of the in-plane bending size effect contributes to an enhancement of our knowledge about this increasingly important, incombustible, damage-tolerant, and environmentally friendly paper fiber-based material. Further, the investigations provide a basis for the determination of an appropriate specimen size and for interpretation of the test result for a future in-plane bending test standard, which does not exist today.

REFERENCES

AICHER, S., AND W. KLÖCK. 2000. Fracture modelling of wood fiber gypsum panel. Pages 469–480 *in* Proc. Int. Conf. on Wood and Wood Fiber Composites, Stuttgart, Germany.

AMERICAN SOCIETY FOR TESTING AND MATERIALS (ASTM).

2003a. Standard test methods for physical testing of gypsum panel products. ASTM C473. ASTM. West Conshohocken, PA.

———. 2003b. ASTM C 1278 Standard specification for fiber-reinforced gypsum panels. ASTM, West Conshohocken, PA.

———. 2004. ASTM C 79 Standard Specification for treated core and non-treated core gypsum sheathing board, ASTM, West Conshohocken, PA.

BATES, D. M., AND D. G. WATTS. 1988. Nonlinear regression analysis and its applications. John Wiley & Sons Inc., New York, NY.

BAZANT, Z. P., AND J. PLANAS. 1998. Fracture and size effect in concrete and other quasibrittle materials. CRS Press, Boca Raton, FL.

EUROPEAN COMMITTEE FOR STANDARDIZATION (CEN). 2003. En 789 "Timber Structures, Test methods—Determination of mechanical properties of wood based panels". En 789, CEN, Brussels, Belgium.

GERMAN INSTITUTE FOR BUILDING TECHNOLOGY (DIBt). 2002. CUAP Large-sized fiber gypsum panels used for walls of prefabricated houses (CUAP). DIBt, Berlin, Germany.

———. 2004. European Technical Approval "Fiber gypsum boards used for planking and lining of components". ETA-03/0050. DIBt, Berlin, Germany.

HUMMEL, H.-U. 2000. Advanced gypsum fiberboard products for high end applications in the building industry. Pages 356–368 *in* Inorganic-bonded wood and fiber composite materials, Vol. 7, Sun Valley, ID.

ICBO EVALUATION SERVICE (ICBO). 1999. Acceptance criteria for nonpaper-faced fiber-reinforced gypsum panels used as an alternate to gypsum board. (ICBO AC 158. ICB) Whittier, CA.

MILLER, D. P., AND M. R. LYNN. 1998. Development and scale up of USG's gypsum fiberboard technology. Pages 4–12 *in* Inorganic-bonded wood and fiber composite materials, Vol. 6, Sun Valley, ID.